Reversible Achiral-to-Chiral Switching of Single Mn–Phthalocyanine Molecules by Thermal Hydrogenation and Inelastic Electron Tunneling Dehydrogenation

Kai Yang,[†] Liwei Liu,[†] Lizhi Zhang,[†] Wende Xiao,[†] Xiangmin Fei,[†] Hui Chen,[†] Shixuan Du,[†] Karl-Heinz Ernst,[‡,§,*] and Hong-Jun Gao[†,*]

[†]Institute of Physics, Chinese Academy of Sciences, Beijing 100190, China, [‡]Empa, Swiss Federal Laboratories for Materials Science and Technology, Uberlandstrasse 129, 8600 Dübendorf, Switzerland, and [§]Institute of Chemistry, University of Zurich, CH-8057 Zürich, Switzerland

ABSTRACT Induction of chirality in planar adsorbates by hydrogenation of phthalocyanine molecules on a gold surface is demonstrated. This process merely lowers the molecular symmetry from 4- to 2-fold, but also breaks the mirror symmetry of the entire adsorbate complex (molecule and surface), thus rendering it chiral without any realignment at the surface. Repositioning of single molecules by manipulation with the scanning tunneling microscope (STM) causes interconversion of enantiomers. Dehydrogenation of the adsorbate by means of inelastic electron tunneling restores the mirror symmetry of the adsorbate complex. STM as well as density functional theory (DFT) calculations show that chirality is actually imprinted into the electronic molecular system by the surface, *i.e.*, the lowest unoccupied orbital is devoid of mirror symmetry.

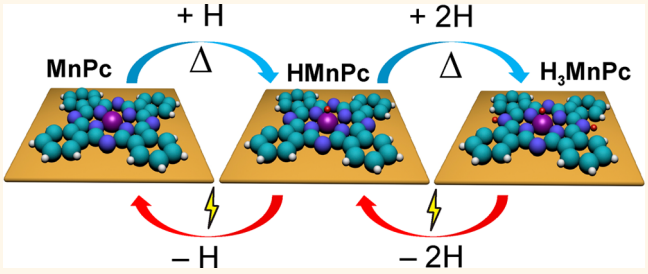

KEYWORDS: chirality · single-molecule manipulation · scanning tunneling microscopy · phthalocyanine · inelastic electron tunneling

Molecular recognition among chiral biomolecules is of fundamental importance to life.[1] It plays a key role for spontaneous resolution into enantiomers during crystallization and for the performance of liquid crystal devices.[2,3] The motivation for better understanding such complex processes as well as the role of chiral surfaces in biomineralization and enantioselective heterogeneous catalysis has led to many studies of chiral recognition at surfaces.[4,5] Taking advantage of its ability of providing submolecular resolution, scanning tunneling microscopy (STM) has been applied to explore molecular chirality at surfaces, including determination of absolute handedness,[6] homochiral recognition,[7] amplification of chirality,[8,9] diasteriomeric recognition,[10–12] and chirality switching.[13–15]

A common feature in molecular adsorption is induction of chirality, *i.e.*, an achiral molecule leads to a chiral adsorbate due to confinement on the surface.[4] In the case of symmetric planar molecules adsorbed parallel to the surface, mirror-symmetry breaking requires an oblique azimuthal orientation.[4] Such misalignment of the molecular mirror plane with respect to the substrate lattice mirror plane leads to a combined molecule-surface system devoid of mirror-symmetry. Translation or rotation of the entire adsorbate complex, *i.e.*, molecule and substrate, will not allow superposition of the enantiomers. Adsorbed on Au(111), Cu(111), and Ag(111), metallo-phthalocyanines (MPcs) (M = Fe, Co, Mn, Cu) maintain their planar configuration, with the molecular planes oriented parallel to the surface.[16–21] Chiral motifs have been reported so far for Cu–phthalocyanine (CuPc) on Ag(100) and Cu(111).[14,22]

Manipulation of single molecules with the STM tip is state-of-the-art nowadays.[23]

* Address correspondence to karl-heinz.ernst@empa.ch, hjgao@iphy.ac.cn.

Received for review October 21, 2013 and accepted January 31, 2014.

Published online January 31, 2014
10.1021/nn405490h

At sufficient voltage bias, tunneling electrons may deposit energy into molecular vibrational modes, leading to molecular surface dynamics and even dissociation.[24−26] Single molecule chemistry performed with the STM on MPcs has been described before.[27] Moreover, dehydrogenation of molecules after excitation with inelastically tunneling electrons emanating from the STM tip has been reported previously.[28,29] A thermal hydrogenation followed by STM-induced dehydrogenation of single molecules has also been demonstrated recently.[30] Here we show that such combined process installs and removes reservedly chirality to/from a single molecular complex.

Since at least one of the molecular mirror planes aligns parallel to a mirror plane of the substrate, no chirality is expressed in the case of manganese phthalocyanine (Figure 1a, MnPc) adsorbed on Au(111). Thermally induced hydrogenation of MnPc on Au(111) lowers the symmetry from 4- to 2-fold, and now the combination of substrate and molecule becomes nonsuperimposable with their mirror images by translation and rotation. By realigning the molecule on the surface *via* STM manipulations, the two mirror-isomeric (enantiomeric) states can be interconverted. Density functional theory (DFT) calculations show that the molecular part of the chiral complex is triply hydrogenated MnPc. Finally, STM-induced dehydrogenation switches the chiral adsorbate into an achiral state again.

RESULTS AND DISCUSSION

After deposition of MnPc molecules (roughly 1% of a close-packed monolayer) on Au(111), subsequent exposure to H_2 at room temperature (600 L, 300 K) and sample cooling to 4.3 K, three different molecular entities are observed by STM (Figure 1b, Supporting Information Figure S1). The plain MnPc molecule shows a cross structure with a central protrusion.[18,31] Other molecules appear also as a cross, but have a depression at the center. This species is identified as HMnPc, with a hydrogen atom coordinated to the Mn atom of MnPc.[18] A third species with only 2-fold symmetry shows a more complicated STM appearance, indicating a significant charge redistribution of the molecular orbitals.

This drastic difference in appearance is attributed to the hydrogenation of MnPc beyond the previously identified HMnPc.[18] As shown below, two additional hydrogen atoms become attached to two opposite outer nitrogen atoms of the macrocycle, *i.e.*, generating a triply hydrogenated MnPc. This species is observed on the fcc as well as the hcp regions of the reconstructed gold surface. Hydrogenation beyond HMnPc is not observed for a closed-packed monolayer, an observation that can be explained as follows: Although H_2 dissociation occurs with rather low probability at steps and defects on gold surfaces, the high dose applied leads to sufficient atomic hydrogen on the surface. However, blocking these active sites with molecules suppresses H_2 dissociation. Exposure of MnPc molecules on Au(111) to gas molecules such as O_2 and CO and their mixtures does not induce a change in STM appearance; hence, impurity effects can be safely excluded here.

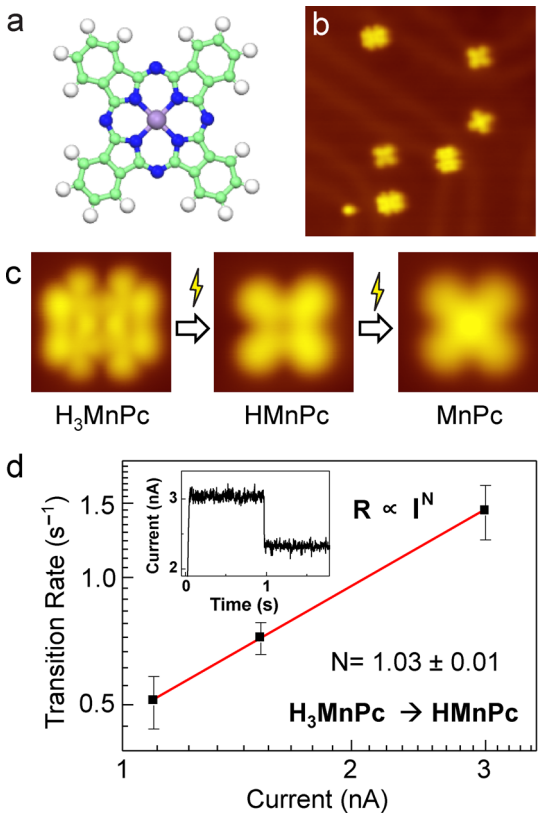

Figure 1. Hydrogenation and dehydrogenation of MnPc on Au(111). (a) Ball-and stick model of MnPc. (b) STM image (17 nm × 17 nm, I = 100 pA, U = 0.1 V) showing three different types of molecular entities after exposure of MnPc/Au(111) to H_2. (c) STM images (2.1 nm × 2.1 nm, I = 100 pA, U = 0.1 V) showing stepwise dehydrogenation from H_3MnPc to HMnPc and to MnPc, induced by inelastic electron tunneling. (d) Transition rate R from H_3MnPc to HMnPc as a function of tunneling current for a fixed bias voltage of 1.15 V. The linear line represents the power-law fit ($R \propto I^N$) with $N = 1.03 \pm 0.01$ indicating a one-electron process. Inset: Tunneling current *versus* time trace measured on the center of the molecule during a dehydrogenation event.

To confirm the extent of hydrogenation of MnPc, STM-induced stepwise dissociation manipulations were performed. That is, substantially higher bias voltages and tunneling currents than used for imaging induce transitions from H_xMnPc to HMnPc and finally to MnPc (Figure 1c). For this procedure, the tip is positioned over the center of a molecule and the bias voltage is applied on the tip with an open feedback loop, while the tunneling current is recorded over time. An abrupt change in the tunneling current marks an action event (Figure 1d, inset), and the nature of the action is analyzed by subsequently acquired STM images and dI/dV spectra. Besides lateral hopping, dehydrogenation is often identified (Figure 1c). To find

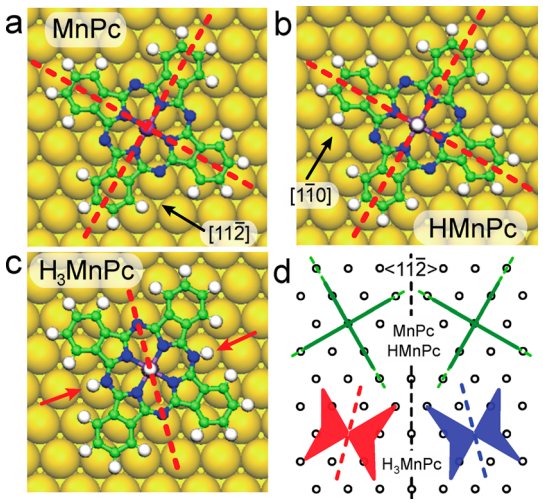

Figure 2. Mirror symmetry breaking by hydrogenation. (a and b) Ball-and stick model of MnPc and HMnPc on Au-(111). Mirror planes (dashed lines) of both species coincide with symmetry planes of the underlying substrate. [11$\bar{2}$] and [1$\bar{1}$0] surface directions are indicated by arrows. (c) Ball-and stick model of H_3MnPc on Au(111). The molecular mirror plane has an oblique tilt to any symmetry planes of the Au substrate underneath, rendering the entire adsorbate complex chiral. The two additional hydrogen atoms at the macrocycle are indicated by red arrows. (d) Comparison of the MnPc/HMnPc alignment (green crosses) with the chiral H_3MnPc alignment (butterflies) on the Au(111) grid (circles).

out how many electrons are involved in this inelastic electron tunneling-induced dehydrogenation of H_xMnPc to HMnPc, 178 switching events were evaluated at different tunneling currents and fixed bias voltage (1.15 V, Supporting Information Figure S2). From the distribution of the residence time for a given current, the rate is deduced.[32] Figure 1d shows the plot of the transition rate R as a function of tunneling current. The rate follows a power-law, $R \sim I^N$, with $N = 1.03 \pm 0.01$, suggesting a one-electron process that drives H_xMnPc to HMnPc.[32,33]

That HMnPc is left after the first dehydrogenation step clearly shows that the H_xMnPc molecule must have more than one additional hydrogen atom. Not many H_xMnPc configurations ($x \geq 2$) with molecular C_{2v} symmetry and the possibility of a transition to HMnPc can be considered. H_2MnPc, for example, on which two hydrogen atoms are bound to the central Mn ion, can be safely excluded, as DFT calculations reveal that the two hydrogen atoms would desorb instantly as H_2. The only possible configuration is therefore H_3MnPc, in which one hydrogen atom is bound to the Mn ion and two others at two opposite outer azamethine N atoms. These nitrogen atoms are targets for hydrogenation without leading to a non-planar configuration. Besides the fact that an additional nodal plane is introduced into the electronic aromatic system, a large delocalized planar electronic structure is still present. Hydrogenation of all four nitrogen atoms would lead again to a 4-fold-symmetric adsorbate and must be excluded from the experimental results. DFT calculations confirm the stability of H_3MnPc and predict the energetic position of the LUMO of H_3MnPc ($\sim$ 0.12 eV with respect to the Fermi level) to be close to the experimental determined position in dI/dV spectra (Supporting Information Figure S3).

Intriguingly, the one-electron dehydrogenation process releases two hydrogen atoms from the macrocycle. A single hydrogen atom left at one nitrogen atom leads to an uneven electron system that strongly disturbs the aromaticity of the ring system. The second dehydrogenation step is therefore expected to occur instantly after the release of the first hydrogen. The chemistry of MnPc can be therefore summarized as follows: hydrogenation occurs at room temperature stepwise to HMnPc and H_3MnPc. These steps can be reversed by excitation with inelastic tunneling electrons at low temperature, leading to stepwise dehydrogenation back to MnPc (Figure 1c).

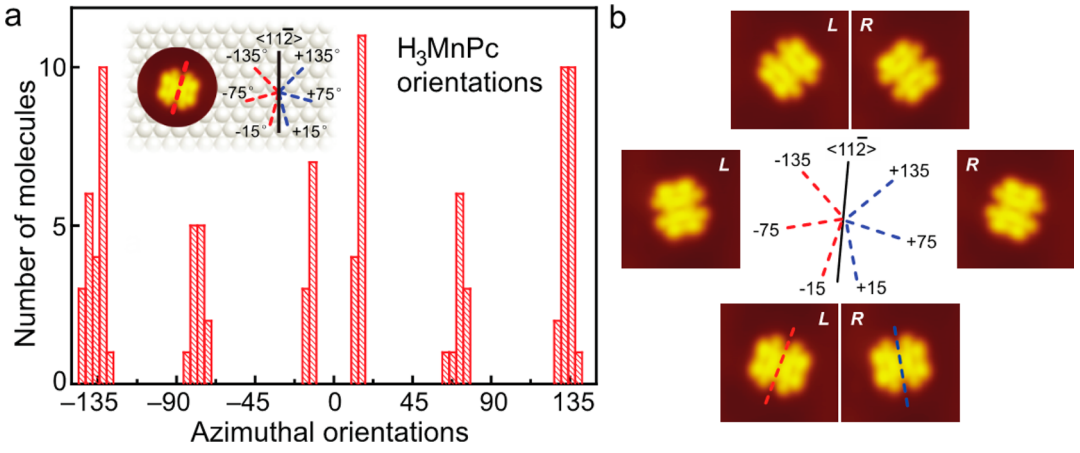

Figure 3. Azimuthal orientations of H_3MnPc on Au(111). (a) Histogram showing distribution of the orientations of H_3MnPc with respect to the ⟨11$\bar{2}$⟩ direction of the Au(111) surface. The six preferential orientations are indicated in the inset. (b) STM images (4.1 nm × 4.1 nm, I = 100 pA, U = 0.1 V) showing the interconversion of six molecular orientations of a single H_3MnPc molecule by lateral manipulation with the STM.

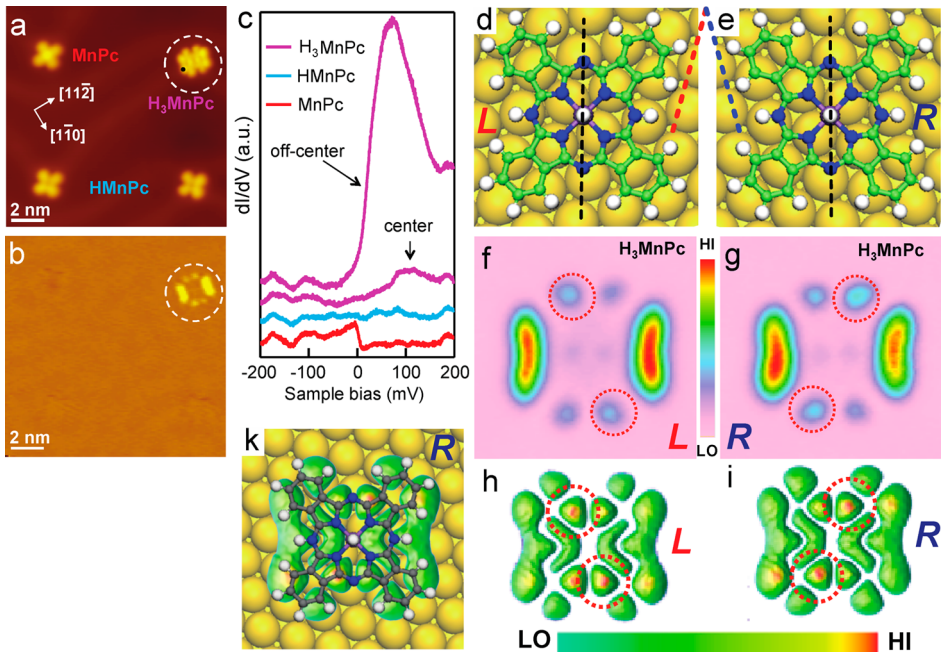

Figure 4. Chiral electronic structure of H_3MnPc on Au(111). (a) STM image (I = 100 pA, U = 0.1 V) of an area containing MnPc, HMnPc, and H_3MnPc (circle) molecules. (b) dI/dV-STM image at U = 100 mV (set point: I = 100 pA, U = −0.1 V) over the same region as shown in (a). At this bias the contrast for H_3MnPc is dominated by its LUMO. (c) dI/dV spectra (set point: I = 0.1 nA, U = −0.2 V) taken at the center of MnPc, HMnPc, H_3MnPc and off-center on H_3MnPc. The off-center spectrum of H_3MnPc exhibits a pronounced broad peak above the Fermi level. This peak is located at 70 mV and represents tunneling into the lowest unoccupied molecular orbital (LUMO). (d and e) DFT optimized adsorption configurations of both enantiomers of H_3MnPc on Au(111). The molecular parts of the adorbate complex enantiomers are aligned. The dashed black lines indicate the C_{2v}-symmetry axis of H_3MnPc. (f and g) dI/dV maps (set point: I = 100 pA, U = −0.2 V) of two H_3MnPc molecules with opposite handedness, showing opposite contrast (circles). (h and i) Calculated dI/dV maps at the peak position of the LUMO of H_3MnPc on Au(111), also showing opposite chiral contrast of the LUMO. (k) Superposition of theoretical dI/dV map and adsorbate complex.

MnPc and HMnPc have C_{4v} symmetry and two of the molecular mirror planes coincide with mirror planes of the substrate, *i.e.*, mirror planes parallel to the ⟨11$\bar{2}$⟩ and ⟨1$\bar{1}$0⟩ surface directions (Figure 2a,b). Hence, rotation by 120° of the HMnPc−surface complex, for example, leads to superposition with its mirror image (Figure 2d, top). Concerning the energetically most favorable adsorption configuration of H_3MnPc, the Mn atom was found to be located over a bridge site of the Au(111) surface with the molecular azimuthal orientation along the Mn−N axis being rotated from the ⟨11$\bar{2}$⟩ directions of Au(111) by 15° (Figure 2c), again, in very good agreement with STM images. Now, the only molecular mirror plane does not coincide with any symmetry of the substrate (Figure 2c), *i.e.*, it is aligned in an oblique fashion with respect to the substrate. Thus, the adsorbate complex is chiral: Only reflection with respect to the ⟨11$\bar{2}$⟩ directions will coincide both enantiomers. Statistical analysis of all alignments of this species reveals six distinct orientations of the entire adsorbate complexes (Figure 3), compatible with two enantiomeric species and their three 120° rotational isomers, as dictated by the C_{3v} symmetry of the underlying substrate. The achiral MnPc and HMnPc species come only in three unique orientations of their rotational isomers. Adding two more H atoms to HMnPc reduces the symmetry of the molecule−substrate system and creates a chiral motif, without any realignment of the molecular frame. Depending on which pair of outer nitrogen atoms becomes hydrogenated, the same prochiral HMnPc may either turn into an R- or an L-enantiomer. By separating the two main parts of the adsorbate complexes, namely, molecule and particular surface site, it is possible to interconvert the two enantiomeric states of H_3MnPc. That is, by dragging the molecule it may be aligned on the Au grid such that the opposite mirror complex (enantiomorph) results. All six distinguished alignments of the chiral adsorbate complex are shown in Figure 3. They were established by repeated STM-tip-induced lateral moves of the same H_3MnPc molecule.

Chirality should be also observable in the electronic structure of the adsorbate complex. This is indeed achieved here by acquiring current-to-voltage differential STM images, so-called dI/dV maps. Taken at the bias voltage dominated by the LUMO of H_3MnPc, they show strong contrast for the fully hydrogenated species, whereas the other two species do not have electronic states at this bias voltage (Figure 4a−c).[18] The dI/dV spectra acquired at the central Mn ion of MnPc show a pronounced Kondo resonance near the Fermi energy (E_F) close to zero bias (Figure 4c).

In contrast, d*I*/d*V* spectra collected at the centers of HMnPc and H_3MnPc are featureless near E_F, suggesting the quenching of the Kondo effect due to hydrogen attachment (Figure 4c). d*I*/d*V* maps of the two H_3MnPc enantiomers reveal strong chiral contrast (Figure 4f,g), *i.e.*, distinctive intensity differences that are opposite mirror images. When the most stable complex derived from DFT is used (Figure 4d,e), the calculated d*I*/d*V* maps show the same asymmetries as observed in the experiment (Figure 4h,i). Note that the electronic asymmetry reflected in the LUMO of the molecule arises from the combination of substrate and molecule. For example, the contrast differences located at the carbon atoms next to the not-hydrogenated outer azamethine nitrogen atoms correlate with good/bad alignments to 3-fold hollow sites of the substrate (Figure 4k and Figures 4d,e and Supporting Information Figure S4). Hence, the asymmetric substrate alignment imposes actually a chiral footprint onto the electronic structure of the molecule.

CONCLUSIONS

Hydrogenation of MnPc to H_3MnPc leads to misalignment of molecular symmetry axes with respect to the substrate surface without moving the molecular frame. This process installs chirality to the otherwise achiral adsorbate complex. A chiral footprint onto the electronic structure, as observed in d*I*/d*V* maps dominated by the LUMO, is the consequence of this process. Interconversion of the enantiomers is possible by STM manipulations that move only the molecule on the surface. Dehydrogenation of single molecules by inelastic electron tunneling switches the chiral complex back into an achiral one.

EXPERIMENTAL AND COMPUTATIONAL DETAILS

Experiments were carried out in an ultrahigh vacuum ($p < 1 \times 10^{-10}$ mbar) low-temperature STM system (Unisoku), equipped with standard surface preparation facilities. The Au(111) surface was prepared by repeated cycles of argon ion sputtering and annealing at 800 K. MnPc molecules (Sigma-Aldrich, 97% purity) were deposited onto the surface by sublimation from a Knudsen-type evaporator held at 580 K, while the substrate was at room temperature (RT). Hydrogen adsorption was performed by dosing 600 Langmuir at RT, followed by sample transfer into the STM at 4.3 K. STM images were acquired in constant-current mode, with the tip at ground potential (positive bias voltages indicate tunneling from the tip to the sample). All experiments were performed with electrochemically etched tungsten tips, which were calibrated with respect to the Au(111) surface state before spectroscopic measurements. d*I*/d*V* spectra were collected by using a lock-in technique with a 0.5 mV_{rms} sinusoidal modulation at a frequency of 973 Hz. The lateral manipulation was carried out by placing the STM tip on top of a molecule, lowering the tunneling resistance down to 8.3 MΩ (I = 600 pA, $U = -5$ mV), and laterally moving the tip. For the IET dehydrogenation, the tip was positioned over the center of a molecule, the feedback was turned off, and then a bias voltage was increased to a larger value (in 50 ms) while the tunneling current *versus* time was recorded.

Ab initio calculations were performed using the VASP implementation of DFT in the projected augmented wave (PAW) scheme and the generalized gradient approximation of Perdew, Burke, and Ernzernhof (PBE) for exchange correlation function,[34−36] including van der Waals (vdW) interaction using Grimme's empirical correction.[37−39] The periodic slab models include four layers of gold, MnPc molecule, and a vacuum layer of 15 Å. Except for the two bottom substrate layers, all atoms are fully relaxed until the net force on every atom is less than 0.01 eV/Å. The energy cutoff of the plane-wave basis sets was set to 400 eV, and a single Γ point is employed for Brillouin zone matrix integrations.

Conflict of Interest: The authors declare no competing financial interest.

Acknowledgment. This work was supported by National Natural Science Foundation of China (grant 20973196, 51210003), National "973" projects of China (grant 2009CB929103), the Chinese Academy of Sciences, and SSC. K.-H.E. acknowledges support from the Swiss Sino Science and Technology Cooperation (SSSTC) and the Swiss National Science Foundation (SNSF).

Supporting Information Available: Additional STM image, IET-induced dehydrogenation statistics, measured and calculated d*I*/d*V* spectra and calculated adsorption configuration and d*I*/d*V* maps. This material is available free of charge *via* the Internet at http://pubs.acs.org.

REFERENCES AND NOTES

1. Siegel, J. S. Homochiral Imperative of Molecular Evolution. *Chirality* **1998**, *10*, 24–27.
2. Pérez-García, L.; Amabilino, D. B. Spontaneous Resolution, Whence and Whither: From Enantiomorphic Solids to Chiral Liquid Crystals, Monolayers and Macro- and Supra-Molecular Polymers and Assemblies. *Chem. Soc. Rev.* **2007**, *36*, 941–967.
3. Lemieux, R. P. Chirality Transfer in Ferroelectric Liquid Crystals. *Acc. Chem. Res.* **2001**, *34*, 845–853.
4. Ernst, K.-H. Molecular Chirality at Surfaces. *Phys. Status Solidi B* **2012**, *249*, 2057–2088.
5. Raval, R. Chiral Expression from Molecular Assemblies at Metal Surfaces: Insights from Surface Science Techniques. *Chem. Soc. Rev.* **2009**, *38*, 707–721.
6. Lopinski, G. P.; Moffatt, D. J.; Wayner, D. D. M.; Wolkow, R. A. Determination of the Absolute Chirality of Individual Adsorbed Molecules Using the Scanning Tunnelling Microscope. *Nature* **1998**, *392*, 909–911.
7. Kühnle, A.; Linderoth, T. R.; Hammer, B.; Besenbacher, F. Chiral Recognition in Dimerization of Adsorbed Cysteine Observed by Scanning Tunnelling Microscopy. *Nature* **2002**, *415*, 891–893.
8. Chen, T.; Yang, W.-H.; Wang, D.; Wan, L.-J. Globally Homochiral Assembly of Two-Dimensional Molecular Networks Triggered by Co-Absorbers. *Nat. Commun.* **2013**, *4*, 1389/1–8.
9. Destoop, I.; Ghijsens, E.; Katayama, K.; Tahara, K.; Mali, K. S.; Tobe, Y.; De Feyter, S. Solvent-Induced Homochirality in Surface-Confined Low-Density Nanoporous Molecular Networks. *J. Am. Chem. Soc.* **2012**, *134*, 19568–19571.
10. Chen, Q.; Richardson, N. V. Enantiomeric Interactions between Nucleic Acid Bases and Amino Acids on Solid Surfaces. *Nat. Mater.* **2003**, *2*, 324–328.
11. Seibel, J.; Allemann, O.; Siegel, J. S.; Ernst, K.-H. Chiral Conflict among Different Helicenes Suppresses Formation of One Enantiomorph in 2D Crystallization. *J. Am. Chem. Soc.* **2013**, *135*, 7434–7437.
12. Roth, C.; Passerone, D.; Ernst, K.-H. Pasteur's Quasiracemates in 2D: Chiral Conflict between Structurally Different Enantiomers Induces Single-Handed Enantiomorphism. *Chem. Commun.* **2010**, *46*, 8645–8647.

13. Comstock, M. J.; Strubbe, D. A.; Berbil-Bautista, L.; Levy, N.; Cho, J.; Poulsen, D.; Fréchet, J. M. J.; Louie, S. G.; Crommie, M. F. Determination of Photoswitching Dynamics through Chiral Mapping of Single Molecules Using a Scanning Tunneling Microscope. *Phys. Rev. Lett.* **2010**, *104*, 178301/1–4.
14. Schaffert, J.; Cottin, M. C.; Sonntag, A.; Karacuban, H.; Bobisch, C. A.; Lorente, N.; Gauyacq, J.-P.; Möller, R. Imaging the Dynamics of Individually Adsorbed Molecules. *Nat. Mater.* **2013**, *12*, 223–227.
15. Parschau, M.; Passerone, D.; Rieder, K.-H.; Hug, H. J.; Ernst, K.-H. Switching the Chirality of Single Adsorbate Complexes. *Angew. Chem., Int. Ed.* **2009**, *48*, 4065–4068.
16. Gao, L.; Ji, W.; Hu, Y. B.; Cheng, Z. H.; Deng, Z. T.; Liu, Q.; Jiang, N.; Lin, X.; Guo, W.; Du, S. X.; *et al.* Site-Specific Kondo Effect at Ambient Temperatures in Iron-Based Molecules. *Phys. Rev. Lett.* **2007**, *99*, 106402/1–4.
17. Zhao, A.; Li, Q.; Chen, L.; Xiang, H.; Wang, W.; Pan, S.; Wang, B.; Xiao, X.; Yang, J.; Hou, J. G.; *et al.* Controlling the Kondo Effect of an Adsorbed Magnetic Ion through Its Chemical Bonding. *Science* **2005**, *309*, 1542–1544.
18. Liu, L. W.; Yang, K.; Jiang, Y.; Song, B.; Xiao, W.; Li, L.; Zhou, H.; Wang, Y.; Du, S.; Ouyang, M.; *et al.* Reversible Single Spin Control of Individual Magnetic Molecule by Hydrogen Atom Adsorption. *Sci. Rep.* **2013**, *3*, 1210/1–510.1038/srep01210.
19. Chang, S.-H.; Kuck, S.; Brede, J.; Lichtenstein, L.; Hoffmann, G.; Wiesendanger, R. Symmetry Reduction of Metal Phthalocyanines on Metals. *Phys. Rev. B* **2008**, *78*, 233409/1–4.
20. Takács, A. F.; Witt, F.; Schmaus, S.; Balashov, T.; Bowen, M.; Beaurepaire, E.; Wulfhekel, W. Electron Transport through Single Phthalocyanine Molecules Studied Using Scanning Tunneling Microscopy. *Phys. Rev. B* **2008**, *78*, 233404/1–4.
21. Gopakumar, T. G.; Brumme, T.; Kröger, J.; Toher, C.; Cuniberti, G.; Berndt, R. Coverage-Driven Electronic Decoupling of Fe-Phthalocyanine from a Ag(111) Substrate. *J. Phys. Chem. C* **2011**, *115*, 12173–12179.
22. Mugarza, A.; Lorente, N.; Ordejón, P.; Krull, C.; Stepanow, S.; Bocquet, M. L.; Fraxedas, J.; Ceballos, G.; Gambardella, P. Orbital Specific Chirality and Homochiral Self-Assembly of Achiral Molecules Induced by Charge Transfer and Spontaneous Symmetry Breaking. *Phys. Rev. Lett.* **2010**, *105*, 115702/1–4.
23. Morgenstern, K.; Lorente, N.; Rieder, K.-H. Controlled Manipulation of Single Atoms and Small Molecules Using the Scanning Tunnelling Microscope. *Phys. Status Solidi B* **2013**, *250*, 1671–1751.
24. Ho, W. Single-Molecule Chemistry. *J. Phys. Chem.* **2002**, *117*, 11033–11061.
25. Stipe, B. C.; Rezaei, M. A.; Ho, W.; Gao, S.; Persson, M.; Lundqvist, B. I. Single-Molecule Dissociation by Tunneling Electrons. *Phys. Rev. Lett.* **1997**, *78*, 4410–4413.
26. Sloan, P. A.; Palmer, R. E. Two-Electron Dissociation of Single Molecules by Atomic Manipulation at Room Temperature. *Nature* **2005**, *434*, 367–371.
27. Li, Z.; Li, B.; Yang, J.; Hou, J. G. Single-Molecule Chemistry of Metal Phthalocyanine on Noble Metal Surfaces. *Acc. Chem. Res.* **2010**, *43*, 954–962.
28. Parschau, M.; Rieder, K.-H.; Hug, H. J.; Ernst, K.-H. Single-Molecule Chemistry and Analysis: Mode-Specific Dehydrogenation of Adsorbed Propene by Inelastic Electron Tunneling. *J. Am. Chem. Soc.* **2011**, *133*, 5689–5691.
29. Kim, Y.; Komeda, T.; Kawai, M. Single-Molecule Surface Reaction by Tunneling Electrons. *Surf. Sci.* **2002**, *502−503*, 7–11.
30. Katano, S.; Kim, Y.; Hori, M.; Trenary, M.; Kawai, M. Reversible Control of Hydrogenation of a Single Molecule. *Science* **2007**, *316*, 1883–1886.
31. Fu, Y.-S.; Ji, S.-H.; Chen, X.; Ma, X.-C.; Wu, R.; Wang, C.-C.; Duan, W.-H.; Qiu, X.-H.; Sun, B.; Zhang, P.; *et al.* Manipulating the Kondo Resonance through Quantum Size Effects. *Phys. Rev. Lett.* **2007**, *99*, 256601/1–4.
32. Stipe, B. C.; Rezaei, M. A.; Ho, W. Inducing and Viewing the Rotational Motion of a Single Molecule. *Science* **1998**, *279*, 1907–1909.
33. Stroscio, J. A.; Celotta, R. J. Controlling the Dynamics of a Single Atom in Lateral Atom Manipulation. *Science* **2004**, *306*, 242–247.
34. Vanderbilt, D. Soft Self-Consistent Pseudopotentials in a Generalized Eigenvalue Formalism. *Phys. Rev. B* **1990**, *41*, 7892–7895.
35. Kresse, G.; Furthmüller, J. Efficient Iterative Schemes for *ab Initio* Total-Energy Calculations Using a Plane-Wave Basis Set. *Phys. Rev. B* **1996**, *54*, 11169–11186.
36. Perdew, J. P.; Burke, K.; Ernzerhof, M. Generalized Gradient Approximation Made Simple. *Phys. Rev. Lett.* **1996**, *77*, 3865–3868.
37. Grimme, S. Semiempirical GGA-Type Density Functional Constructed with a Long-Range Dispersion Correction. *J. Comput. Chem.* **2006**, *27*, 1787–1799.
38. Bučko, T.; Hafner, J.; Lebègue, S.; Ángyán, J. G. Improved Description of the Structure of Molecular and Layered Crystals: *Ab Initio* DFT Calculations with van der Waals Corrections. *J. Phys. Chem. A* **2010**, *114*, 11814–11824.
39. Tonigold, K.; Gross, A. Adsorption of Small Aromatic Molecules on the (111) Surfaces of Noble Metals: A Density Functional Theory Study with Semiempirical Corrections for Dispersion Effects. *J. Phys. Chem.* **2010**, *132*, 224701.